

Supplementary Information

Bouncing and 3D Printable Hybrids with Self-healing Properties

Francesca Tallia^a, Laura Russo^b, Siwei Li^{a,c}, Alexandra L.H. Orrin^{a,1}, Xiaomeng Shi^{a,d}, Shu Chen^{a,2}, Joseph A.M. Steele^e, Sylvain Meille^f, Jérôme Chevalier^f, Peter D. Lee^{d,g}, Molly M. Stevens^{a,c,e,h}, Laura Cipolla^{b,*}, Julian R. Jones^{a,*}

^a *Department of Materials, Imperial College London, South Kensington Campus, London, SW7 2AZ, UK*

^b *Department of Biotechnology and Biosciences, University of Milano-Bicocca, Piazza della Scienza 2, Milano, 20126, Italy*

^c *Department of Bioengineering, Imperial College London, South Kensington Campus, London, SW7 2AZ, UK*

^d *Research Complex at Harwell, Rutherford Appleton Laboratory, Harwell, Oxfordshire, OX11 0FA, UK*

^e *Department of Medical Biochemistry and Biophysics, Karolinska Institutet, Scheeles väg 2, 17177 Stockholm, Sweden*

^f *Université de Lyon, INSA Lyon, MATEIS CNRS UMR5510, Villeurbanne, F-69621, France*

^g *School of Materials, The University of Manchester, Oxford Road, Manchester, M13 9PL, UK*

^h *Institute of Biomedical Engineering, Imperial College London, South Kensington Campus, London, SW7 2AZ, UK*

* Corresponding Authors: julian.r.jones@imperial.ac.uk, laura.cipolla@unimib.it

¹ Present address: Withers & Rogers LLP, 4 More London Riverside, London, SE1 2AU, UK

² Present address: Crystallography, Department of Biological Sciences and ISMB, University of London, Malet Street, London, WC1E 7HX, UK

Experimental Section

Materials. All chemicals were purchased from Sigma-Aldrich and VWR, UK and Italy, and all cell culture reagents were obtained from Invitrogen and Sigma-Aldrich, UK, unless specified otherwise. Reactions were carried out using commercially available starting materials and solvents without any further purification.

PCL oxidation. Polycaprolactone diol (PCL-diol, M_n 530 Da, 3.0 g, 5.66 mmol) was dissolved in CH_3CN (45.70 mL). Satd. aq. NaHCO_3 (12.30 mL), 0.5 M aqueous solution of KBr (4.53 mL, 2.26 mmol), and a 0.1 M solution of TEMPO in CH_3CN (11.32 mL, 1.13 mmol) were sequentially added drop-wise. The reaction was stirred at R.T. till complete dissolution of all reagents, then 5 vol.% aq. NaOCl (74.04 mL) was dropped portion-wise over a period of 24 h. After completion, the reaction was quenched by adding drop-wise 37 vol.% aq. HCl till $\text{pH} \leq 3$. After 1 h, the solution was concentrated under vacuum. The aqueous residue was extracted three times with ethyl acetate. The collected organic layers were dried over anhydrous Na_2SO_4 , filtered and concentrated to dryness, affording the corresponding dicarboxylic acid (PCL-diCOOH).

The reaction was monitored through thin-layer chromatography (TLC) on Silica Gel 60 F254 plates (Merck) charring with a solution containing concd. $\text{H}_2\text{SO}_4/\text{EtOH}/\text{H}_2\text{O}$ in a ratio of 5:45:45 or with an oxidant mixture composed of $(\text{NH}_4)\text{Mo}_7\text{O}_{24}$ (21 g), $\text{Ce}(\text{SO}_4)_2$ (1 g), concd. H_2SO_4 (31 mL) in water (500 mL). The mobile phase consisted of a mixture of acetonitrile and ethanol in a volume ratio of 9:1 respectively. Solvents were dried over molecular sieves at least 24 h prior to use.

The completion of the oxidation was verified (data not shown) by comparing PCL-diol and PCL-diCOOH through: (i) Liquid-state $^1\text{H-NMR}$ Spectroscopy performed through a 400 MHz Bruker spectrometer running with Top Spin software. Sample preparation required the dissolution of 25 mg of polymer in approximately 0.7 mL of deuterated chloroform (CDCl_3). This solution was then syringed into a 5 mm diameter borosilicate glass NMR tube for the analysis in the spectrometer. The experimental parameters were set to take 16 scans in the range of chemical shift 0-12 ppm (chemical shifts are reported in ppm downfield from TMS as an internal standard); (ii) Matrix-assisted Laser Desorption/Ionisation – Time-of-flight (MALDI-ToF) Mass Spectroscopy (Micromass MALDI

MicroMX-ToF). Samples were prepared by dissolving the polymer in tetrahydrofuran (THF) at a concentration of 10 mg mL^{-1} and mixing it in a 50:50 vol.% with 2,5-dihydroxybenzoic acid (DHB) used as matrix. The mass spectrum was then collected in the mass range 300-2000 Da using the reflectron positive mode. Further qualitative confirmation was obtained from Fourier-Transform Infrared Spectroscopy in Attenuated Total Reflectance mode (ATR-FTIR) mode using a Thermo Scientific Nicolet iS10 FTIR equipped with Smart Golden Gate for Single-Reflection Diamond ATR Analysis with OMNIC software. Analysis was carried out by placing a drop of polymer (which showed a gel consistency) on the ATR crystal. The experimental parameters were set to take 64 scans at a resolution of 4 LP mm^{-1} to form spectra in absorbance between the range $4000\text{-}400 \text{ cm}^{-1}$ (in the mid-infrared range, $4000\text{-}200 \text{ cm}^{-1}$).

Hybrid synthesis. Hybrid samples containing SiO_2 as inorganic component, PTHF and PCL-diCOOH as organic phases were prepared following the three-pot reaction shown in Fig. 1a.

Preparation of the organic precursor solution. In a typical synthesis, PCL-diCOOH (1 mol) prepared as previously described was dissolved in anhydrous THF at R.T. at a concentration of 50 mg mL^{-1} to prepare bulk samples and of 100 mg mL^{-1} to print porous scaffolds. Under continuous stirring, GPTMS (2 mol) was added. After 30 minutes, boron trifluoride diethyletherate ($\text{BF}_3 \cdot \text{OEt}_2$, 0.5 mol) was added to the solution to activate the epoxide ring of GMPTS and, consequently, initiate the polymerisation of THF, leading to the formation of a GPTMS–PTHF–PCL-diCOOH network dissolved in the remaining non-polymerised THF. The polymer solution was allowed to stir for 1.5 h. $^1\text{H-NMR}$ (with same machine and setup described to check PCL oxidation) was used to verify the opening of the epoxide ring and the appearance of the new polymer phase: for each analysis $\sim 50 \mu\text{L}$ of organic precursor solution were dissolved in $\sim 0.7 \text{ mL}$ of CDCl_3 . Two spectra were compared, the first was collected before $\text{BF}_3 \cdot \text{OEt}_2$ addition and the second was collected after $\text{BF}_3 \cdot \text{OEt}_2$ addition just before mixing with the solution containing inorganic precursors.

The mechanism of reaction was verified by preparing alternative organic precursor solutions. In a first series of experiments one or two reagents were removed from the original solution. Particularly, the following systems were investigated: THF and $\text{BF}_3 \cdot \text{OEt}_2$; THF, PCL-diCOOH and $\text{BF}_3 \cdot \text{OEt}_2$; THF,

GPTMS and $\text{BF}_3 \cdot \text{OEt}_2$. In a second series of experiments, starting from the tri-component system composed of THF, GPTMS and $\text{BF}_3 \cdot \text{OEt}_2$, one reagent at a time was substituted by another one with similar functionalities. Particularly, the following variations were investigated: scandium(III) triflate ($\text{Sc}(\text{OTf})_3$) instead of $\text{BF}_3 \cdot \text{OEt}_2$ as catalyst; glycidyl methyl ether (GME) instead of GPTMS as source of epoxide ring; trimethoxy(propyl)silane (TMPS) instead of GPTMS as silica source; tetrahydropyran (THP) instead of THF as monomer and solvent. In each reaction, the concentrations (i.e. molar ratios) among reagents, synthesis conditions and $^1\text{H-NMR}$ follow-up were unvaried from the original hybrid system.

Preparation of the inorganic sol. TEOS, the silica precursor, was hydrolysed in deionised water by 1 M hydrochloric acid (1 M HCl). Five different TEOS/PCL-diCOOH wt.% (0/100, 60/40, 70/30, 80/20, 90/10) were used in order to prepare five different hybrid compositions, that were respectively identified as Si0-CL, Si60-CL, Si70-CL, Si80-CL and Si90-CL. Water content was calculated as the sum of the stoichiometric amounts needed to hydrolyse both TEOS and GPTMS, which means $\text{H}_2\text{O}:\text{TEOS} = 4:1$ molar ratio and $\text{H}_2\text{O}:\text{GPTMS} = 3:1$ molar ratio; 1 M HCl was added at a concentration of 1 M HCl: $\text{H}_2\text{O} = 1:3$ vol.%. The resultant mixture was vigorously stirred for 1-1.5 h to induce complete hydrolysis.

Preparation of the hybrid sol. When the two separate solutions were fully reacted, the inorganic precursor solution was added drop-wise to the organic precursor solution and stirred at R.T. for 30 minutes in a sealed container to form the hybrid sol.

Formation of bulk samples. In order to obtain bulk samples, the hybrid sol was cast into cylindrical polytetrafluoroethylene (PTFE) containers (internal $\varnothing = 130$ mm) and placed at 40°C for ageing (3 days with the container sealed) and drying (gradual loosening of the lid over 10-28 days to avoid cracking during solvent evaporation and mutual arrangement of SiO_2 , PTHF and PCL-diCOOH chains). When dried, samples were in the shape of discs, with final dimensions determined by the shrinkage inherent to the sol-gel process. Samples were removed from the oven and immersed in deionised water for 10 s to remove reaction by-products.

3D extrusion printing of porous scaffolds. Si80-CL composition was used for 3D extrusion printing directly from the sol-gel. To obtain porous scaffolds, the hybrid sol was stirred without a lid to

evaporate part of the residual THF and accelerate the gelation process, until a suitable viscosity was reached that allowed removal of bubbles, via an ultrasound bath, and the transfer into a 3 mL luer-lock plastic syringe (VWR International, UK), equipped with a tapered tip for 3D printing (Nordson EFD, UK). Residual air was removed by tilting the syringe with the nozzle upwards and manually pressing the plunger until the sol started to be extruded. The syringe was then placed into a robocasting machine (“Robocaster”, 3d Inks LLC, USA), connected to a computer equipped with the software “Robocad” (3d Inks LLC, USA), which controlled the printing of porous scaffolds following a specific CAD file. The gelation process continued in the syringe, gradually increasing the ink viscosity, until the optimal viscosity to be used as an ink for 3D extrusion printing was achieved. At this point, the printing window was ~1 h, during which 3D porous scaffolds were printed following an orthogonal grid-like pattern so that each layer consists of a linear array of parallel struts and alternating layers are oriented at 90° to each other and subsequent arrays are aligned with the previous layer without any shift (Video S3). The following printing parameters were used: conical nozzle with internal diameter of 0.20 mm, speed of 10 mm s⁻¹, z-spacing of 0.21 mm and strut spacing of 0.60 mm. Cubic scaffolds with dimensions ranging between 9.6-12.0 mm were printed and, while still wet, were placed in Nalgene polymethylpentene (PMP) containers at 40°C for ageing (3 days with the container sealed) and drying (gradual loosening of the lid over 4-7 days). Scaffolds were finally immersed in deionised water for 10 s to remove reaction by-products.

Characterisation of the hybrid network.

The final I/O ratio was determined through TGA for each hybrid composition. The total organic content derived from PCL-diCOOH, the organic portion of GPTMS introduced in the starting solution and PTHF generated by in situ CROP; the inorganic content consisted of the silica derived from TEOS and GPTMS. DSC/TGA (Netzsch Jupiter STA 449C) was used on powders (10-15 mg), ground with a pestle and mortar and weighed out into a platinum crucible. The soft nature of Si0-CL and Si60-CL hybrids did not allow grinding, therefore the test was performed using small bulk pieces of similar mass. The range of analysis was 20-800°C with a heating rate of 10°C min⁻¹ in an atmosphere of continuously flowing air. Weight loss was due to the burning-out of organic phase.

ATR-FTIR was carried out on hybrids (with the same setup described for PCL oxidation) to determine

the relative change in functional groups attributed to the inorganic and organic components when comparing the hybrids of different inorganic/organic contents. Samples were in powder form, except for Si0-CL and Si60-CL hybrids.

Si80-CL hybrid was used in Bright Field Transmission Electron Microscopy (BFTEM) and High Angle Annular Dark Field (HAADF) Scanning Transmission Electron Microscopy (STEM) analysis using a JEOL 2100F scanning/transmission electron microscope operated at 200 kV, fitted with an Electron Dispersive X-ray Spectrometer (EDX) X-MaxN Silicon Drift Detector with a detector sizes of 80 mm². The bulk hybrid sample was embedded in a Quetol-based resin of 8.75 g Quetol, 13.75 g nonenyl succinic anhydride, 2.5 g methyl acid anhydride, and 0.62 g benzyl dimethylamine (all from Agar Scientific, UK). After curing at 60°C for 24 h, thin sections (80 nm) were cut directly into a water bath using an ultramicrotome with a diamond knife with a wedge angle of 35°. Sections were immediately collected on bare, 300 mesh copper TEM grids (Agar Scientific, UK), dried and kept under vacuum for TEM analysis.

Mechanical testing of bulk samples. Rectangular specimens for tensile tests, DMA and stress-relaxation tests were cut from the hybrid discs according to ASTM D1708–13.¹⁵ Samples of 45×10 mm were obtained to enable an exposed length of 25 mm and 10 mm to grip the sample at each end. The thickness was determined by the shrinkage of the sol-gel hybrid material during the drying step, but it resulted being in the range 0.6-2 mm. Tensile tests and DMA were performed on the five investigated compositions, whereas stress-relaxations tests were done on Si0-CL and Si80-CL selected compositions.

Uni-axial tensile testing was carried out using a Bose Electroforce Series III machine equipped with WinTest[®] 7 software, fitted with a 220 N load cell, set in displacement control at a rate of 1 mm min⁻¹ until failure. For each sample, it was verified that the fracture section was localised between the grips and no necking was observed. True strain (ε^*) and true stress (σ^*) were calculated from Equation (1) and (2) respectively:

$$\varepsilon^* = \ln(1 + \varepsilon_c) \quad (1)$$

$$\sigma^* = \sigma_c (1 + \varepsilon_c) \quad (2)$$

where σ_c is the conventional stress calculated as the ratio between the force and the nominal cross-section area and ε_c is the conventional strain calculated as the ratio between the actual displacement and the initial length of the sample ($n = 5$). The standard sign convention for tensile testing was used, i.e. force/stress and displacement/strain positive values. Equation (1) and (2) are valid when the volume is constant (which is the case of plasticity or when the Poisson's ratio is close to 0.5) and before necking. True stress and true strain give a more accurate representation of the material response to loading and are particularly important when testing materials which can undergo large homogeneous deformations before fracture, as the hybrids materials of the present work. Modulus of toughness (U_T) was calculated by measuring area underneath the tensile stress-strain curve (where ε^* is unitless) using Origin Software (OriginLab Corporation, USA).

DMA analysis was carried out using the same Bose Electroforce Series III machine, fitted with a 22 N load cell, at 12 frequencies along a log scale between and including 0.01 Hz and 10 Hz. To compare hybrid compositions, the test was performed in displacement control, with dynamic amplitude for each sample set to 20 % of the average deformation at fracture that had been obtained from tensile testing ($n = 4$). The WinTest[®] DMA software allowed the calculation of the storage modulus (E' , indicative of elastic behaviour) and loss modulus and loss tangent (E'' and $\tan(\delta)$ respectively, indicative of dissipative behaviour).

Stress-relaxation tests were carried out using the same Bose Electroforce Series III machine, fitted with a 22 N load cell. The data were collected with samples loaded to 50 % of their ε_c at fracture (obtained from tensile testing) and held under constant strain for 1 h ($n = 5$); the machine was set to bring the samples to the desired strain level in 1 s.

Self-healing assessment. Specimens with the same geometry used for tensile testing were used to assess the self-healing ability of the SiO₂/PTHF/PCL-diCOOH hybrids. Qualitative evaluation was carried out with optical microscope (Olympus BX51 Optical Microscope coupled with Olympus Stream Essentials 1.8 software, used in back lighting mode), by comparing images taken immediately after creating a defect and after a period of "healing" at R.T.. For materials with lower inorganic content (Si0-CL, Si60-CL, Si70-CL), the recovery period was 5 s, following defects created using a

needle inserted into the side of the samples. This approach could not be used on hybrid compositions with higher inorganic fractions (Si80-CL and Si90-CL), so defects were created by making a small notch on the sample surface with a needle and then compressing the sample until a partial internal crack appeared. The recovery time allowed in these cases was 24 h.

Scanning electron microscopy (SEM, JEOL 6010 LV, secondary electron imaging (SEI), 20 kV voltage, working distance between 13-17 mm) was used to capture the healing process of a crack generated on a Si0-CL sample. The defect was created on the sample and allowed to only partially heal at R.T. by bringing together the two counterparts pieces so that only the lower portions of the re-joining surfaces were in contact. The healing process was stopped through coating the sample with a 10 nm layer of chromium for SEM imaging.

Tensile testing as previously described was used to quantitatively evaluate the self-healing ability on Si0-CL hybrids (n = 5): samples were tested in tension to fracture, after which the fractured pieces were brought back together immediately after the test, left healing at R.T. and humidity = 53 ± 5 % for 24 h and then re-tested in tension up to fracture. The healing efficiency (η) was calculated from Equation (3):

$$\eta = \frac{f_{Healed}}{f_{Pristine}} \cdot 100\% \quad (3)$$

Where $f_{Pristine}$ is ε^* or σ^* calculated from the first tensile test and f_{Healed} is ε^* or σ^* calculated after 24 h healing.

Characterisation of the scaffold architecture.

Helium pycnometry (Ultrapycnometer-1000, Quantachrome Corporation) was used to measure the skeletal density (ρ_{sk}) of the hybrid materials (n = 20). ρ_{sk} was needed to calculate the percentage porosity in the scaffold with Equation (4):

$$\%P = 100\% \cdot \left(1 - \frac{\rho_{sc}}{\rho_{sk}}\right) \quad (4)$$

where ρ_{sc} is the scaffold density calculated geometrically (scaffold mass over volume, including pores) (n = 5).

μ CT and SEM were used to investigate the scaffold 3D architecture.

μCT was used to analyse channel size distribution and strut width distribution. The scaffolds, together with a silica glass fibre (fixed on the sample stage to calibrate the X-ray attenuation) were scanned using a commercial μCT device (Phoenix X-ray Systems and Services GmbH, Wunstorf, Germany) at 70 kV and 140 μA, and with voxel dimensions of 9.5 μm. The 3D rendering images of child volumes of scaffolds and quantification were obtained using Avizo 9.0 (Visualization Science Group, Merignac Cedex, France) (n = 6). The segmentation process and quantification steps were applied to the μCT as follows:^{2S, 3S}

1. A 3×3×3 median filter was applied to remove noise;
2. Images were normalised with respect to the attenuation of silica glass fibre;
3. Global thresholding was applied to the normalised images to produce a binary (solid/air) image.
4. A distance map was applied to identify the centre line of the struts, then the local distance from the centre points to the wall was calculated to determine the strut and channel size distributions.

SEM imaging (JEOL 6010 LV, SEI, 20 kV accelerating voltage, working distance between 13-17 mm) was performed on top surface and on the horizontal and vertical sections (which were exposed by manually cut the scaffolds with a sharp blade). Samples were previously coated with a 10 nm layer of chromium in order to make them conductive. SEM images were analysed with ImageJ software to further evaluate channel and strut size distributions.

Mechanical testing on scaffolds. Cubic 3D porous scaffolds (5×5×5 mm) were tested. Uni-axial compression testing to failure was carried out using a Bose Electroforce Series III machine, fitted with a 440 N load cell, set in displacement control at a rate of 0.5 mm min⁻¹. Mean values and corresponding standard deviation of true strain (ϵ^*) and true stress (σ^*) at failure were calculated from Equation (1) and (2) respectively (n = 5), where the standard sign convention for compression testing was used, i.e. force/stress and displacement/strain negative values. Modulus of toughness (U_T) was calculated by measuring area underneath the compression stress-strain curve (where ϵ^* is unitless) using Origin Software (OriginLab Corporation, USA). Cyclic compression testing was performed with the same machine but scaffolds were subject to 10 cycles, all in equal conditions. The experiment was strain-controlled in order to compress each sample up to 20 % of its initial height; both the loading and

unloading steps were performed at an equal speed of 0.5 mm min^{-1} ; a dwell time of 30 s was programmed between each cycle to let the sample recover the deformation after each loading cycle. In all tests scaffolds were loaded in the direction perpendicular to the plane of deposition. DMA analysis was carried out using the Bose Electroforce Series III machine, fitted with a 220 N load cell, at 16 frequencies along a log scale between and including 0.01 Hz and 10 Hz. The tests were performed in displacement control and repeated in three different ranges of strain (ϵ_c): the displacement was set to (i) 1-5 %, (ii) 5-10 % and (iii) 10-15 % of the initial sample height, respectively ($n = 6$). The WinTest[®] DMA software allowed the calculation of the storage modulus (E') and loss modulus and loss tangent (E'' and $\tan(\delta)$ respectively).

Biodegradation of scaffolds. Phosphate-buffered saline (PBS) solution was chosen for biodegradation studies. PBS was prepared by dissolving a 5 g solid tablet (Gibco[®], Thermo Fisher Scientific, Hemel Hempstead, UK; composition: 10 mM sodium phosphates, 140 mM NaCl, 2.68 mM KCl) in 500 mL of deionised water and the final pH was verified to be 7.45. Cubic Si80-CL scaffolds (5×5×5 mm) were soaked in PBS at body temperature (37°C) for 7 days under constant agitation at 120 rpm. Scaffolds degradation was tested using a ratio between the scaffold mass and the PBS volume of 1.5 mg mL^{-1} , normally suggested for testing apatite formation on bioactive glasses in SBF.⁴⁵ The following assessments were performed:

- Macroscopic observation during the test allowed verification of the presence of any defects or visible degradation of the scaffolds;
- Mass loss, measured by weighing the scaffolds before the test and after having been completely dried at RT in air after soaking ($n = 4$);
- Inductively Coupled Plasma Optical Emission Spectroscopy (ICP-OES) on the remaining PBS solution to evaluate the Si dissolution: the samples of solution were analysed without any dilution ($n = 4$) at the 7 day time point; the analysis was done calibrating the machine with a set of Si standards at 0-0.1-0.5-1-2-5-20 $\mu\text{g mL}^{-1}$;
- DSC/TGA (with the same setup previously described) to evaluate the changes in the I/O ratio after the soaking. To run the test, Si80-CL scaffolds were dried at RT after the immersion in PBS, then

ground with a pestle and mortar. DSC/TGA was also run on powders derived from non-soaked Si80-CL scaffolds to obtain a reference pre-soaking I/O ratio;

- SEM of the scaffold surface using both JEOL 6010 LV SEM (for low magnification imaging, SEI, 20 kV voltage, working distance between 13-17 mm) and Leo Gemini 1525 FEGSEM (for high magnification imaging, InLens detector, 3-5 kV voltage, working distance 6-9 mm) to check the effect of the immersion on the morphology;
- Uni-axial compression testing to failure was repeated with the same setup described (n = 5). After soaking for 7 days in PBS, the scaffolds were not dried but were compressed immediately after being taken out from the solution in order to simulate as close as possible the test in wet environment.

A parallel experiment consisting of soaking Si80-CL scaffolds in PBS (7 days, 37°C and 120 rpm) at a higher concentration (15 mg mL⁻¹) was run in order to allow the use of ¹H-NMR to evaluate the nature of any organic phase degraded in solution (n = 2). For each sample, the mother liquors containing degradation products were freeze-dried (Scanvac CoolSafe 110-4, Labogene) in order to remove the water; the residues were then suspended in ~0.7 mL CDCl₃ (in which both PCL-diCOOH and PTHF are soluble) and the solids (residual salts from PBS) were removed by filtration. The obtained clear solution was analysed by ¹H-NMR with the same setup previously described. For comparison, the same experiment was run on the PCL-diCOOH freshly prepared as described above.

In vitro cartilage cell culture. ATDC5 murine chondrogenic cell line (ATCC, UK) was culture expanded in basal DMEM (Dulbecco's Modified Eagle Medium) supplemented with 5 vol.% FCS (foetal calf serum), 100 unit mL⁻¹ penicillin, 100 µg mL⁻¹ streptomycin and 1× ITS liquid supplement (10 µg mL⁻¹ insulin, 5.5 µg mL⁻¹ transferrin and 5 ng mL⁻¹ selenite). Cells were passaged upon confluence using 500 µg mL⁻¹ trypsin-EDTA (ethylene diamine tetra-acetic acid).

Cell seeding and culture on 3D scaffolds. For cell attachment, viability and chondrogenic differentiation studies, Si80-CL scaffolds (5×5×2.5 mm) were sterilised with 70 vol.% ethanol and washed in Phosphate Buffered Saline solution (PBS). ATDC5 cells were harvested and suspended in basal media at a concentration of 2×10⁶ cells in 5 mL. Cell suspension was added to each sterile 50

mL Falcon tube containing one 3D scaffold. The tubes were placed in standard incubator (humidified atmosphere at 37°C, 5% CO₂ and 21% O₂) for 2 h with gentle agitation every 30 minutes to allow diffused cell adhesion. The basal media was then replaced with chondrogenic media consisted of DMEM supplemented with 10 ng mL⁻¹ rhTGF-β3 (100-36E, PeproTech, UK), 100 μM L-Ascorbic acid 2-phosphate, 10 nM dexamethasone and 1× ITS liquid supplement.^{5S, 6S} Chondrogenic differentiation and cartilaginous matrix formation on PCL scaffolds with similar structure were also investigated as comparison. PCL scaffolds were produced by direct writing melt electrospinning^{7S} on a custom apparatus (Hutmacher Lab, QUT, Australia). PCL (45 kDa, Sigma-Aldrich) was extruded at 65°C by compressed air through a 23G blunt needle, positioned 7.5 mm above a motorised stage and charged with a positive potential of 4.5 kV. The stage was positioned beneath the stationary syringe at 100 mm min⁻¹ by custom G-code script running on Mach3 software. Five layers of orthogonal lattice with struts spaced at 0.4 mm intervals were deposited, producing sheets 1 mm in thickness (Fig. S10).

Analysis of cell viability. Viability of ATDC5 cells on the 3D scaffolds following 1, 7 and 14 days of culture was determined using a colorimetric water-soluble tetrazolium salt (WST-1) proliferation assay. Cell-seeded scaffolds were submerged in 5 mL of WST-1 reagent (1:10 dilution in DMEM, Roche Diagnostic, West Sussex, UK). 100 μL was aspirated in triplicate from each sample following 2 h incubation and the optical density was measured spectrophotometrically at 440 nm (n = 3 at each time point).

Immunohistochemical analysis of cell attachment and chondrogenic differentiation. Cell-seeded scaffolds were collected on day 3 and 21 for immunohistochemical analysis of cell attachment and cartilaginous matrix formation respectively. 4% paraformaldehyde (PFA) fixed samples were permeabilised with buffered 0.5% Triton X-100 in PBS (300 mM sucrose, 50 mM NaCl, 3 mM MgCl₂, 20 mM Hepes and pH 7.2). Following blocking with 10 mg mL⁻¹ BSA (Bovine Serum Albumin) in PBS, samples were incubated with relevant primary antiserum at 4°C overnight. This was followed by 1 h incubation with Alexa Fluor® 488-conjugated secondary antibody. Isotype controls were performed in all immunohistochemistry procedures and no staining was observed. Cytoskeletal marker anti-Vimentin antibody (rabbit polyclonal, IgG, Abcam, Cambridge, UK) was used at a dilution of 1:500 in 10 mg mL⁻¹ BSA. Chondrogenic differentiation and cartilaginous matrix markers, anti-Sox9,

Aggrecan, Collagen Type II, Collagen Type I and Collagen Type X antibodies were used at dilutions of 1:150, 1:150, 1:500, 1:1000 and 1:100 respectively in 10 mg mL⁻¹ BSA. F-actin was labelled using CytoPainter F-actin staining kit (Abcam, Cambridge, UK) following the manufacturer's instruction. Briefly, Alexa Fluor® 568-conjugated phalloidin (1:1000 dilution in 10 mg mL⁻¹ BSA) was added simultaneously with the secondary antibody during the incubation period. All samples were counter-stained with DAPI (0.1 µg mL⁻¹ in PBS).

Confocal microscopy. Samples were imaged under confocal microscopy (Leica SP5 MP laser scanning confocal microscope, Leica Microsystems, Germany) and composite images were reconstructed using ImageJ software.

qPCR gene expression analysis. Day 21 cell-seeded scaffolds (n = 3) were lysed for RNA extraction using Qiagen RNeasy kit (Qiagen, Manchester, UK) following manufacturer's instructions. Following treatment with DNase-1 reagent and RNA samples were reverse-transcribed using the SuperScript® VILO™ cDNA synthesis kit (Invitrogen, UK). SYBR green based qPCR assays were performed using the QuantStudio™ 6 Flex system (Thermo Fisher, UK) for the analysis of cartilage related gene expression, including *Sox9* (F: 5'- ctgaagggtactgactggac -3'; R: 5'- gaggaggaatgtggggagtc -3'), *Aggrecan* (F: 5'- aggagtggtactgctggtg -3'; R: 5'- tctcactccaggaactcgt -3'), *Col2a1* (F: 5'- agtcaaggagatcgtggtg -3'; R: 5'- cgtcgtgctgtctcaagta -3'), *Coll1a1* (F: 5'-gagaagtctcaagatggtggc -3'; R: 5'- gcggggtcggagccctcgtt -3') and *Coll10a1* (F: 5'- cataaagggccacttgcta -3'; R: 5'- caggaatgcctgttctcct -3'). The expression of genes of interest was normalised to the housekeeping gene GAPDH (F: 5'- ggggtggagccaaacgggtc -3'; R: 5'-ggagttgctgttgaagtcgca -3'). The relative transcript levels of genes of interest were analysed using the comparative C_T (ΔΔC_T) method. For each gene of interest, the group with the highest expression was assigned to a value of 1. The range of relative transcript levels of the genes of interest was plotted as bar graphs and statistical analysis was performed at the level of ΔC_T.

Quantification of sulphated glycosaminoglycan (sGAG). Total sGAG synthesised by cells following 21-day culture on Si80-CL and PCL scaffolds (n = 3) was determined using the dimethylmethylene blue (DMMB) assay. Cell-seeded scaffolds were digested overnight at 60°C in 0.7 U papain (prepared in papain buffer consisting 8.2 mg mL⁻¹ sodium acetate, 37 mg mL⁻¹ disodium EDTA and 0.79 mg mL⁻¹ cysteine hydrochloride in potassium phosphate solution containing 27.2 mg mL⁻¹ monobasic

potassium phosphate and 34.8 mg mL^{-1} dibasic potassium phosphate, pH 6.4). The digested samples were centrifuged and $20 \text{ }\mu\text{L}$ of the diluted extract (1:10 dilution in papain buffer) was then mixed with $200 \text{ }\mu\text{L}$ DMMB reagent ($16 \text{ }\mu\text{g mL}^{-1}$ DMMB, 2 mg mL^{-1} sodium formate, 0.5 vol.% ethanol and 0.2 vol.% formic acid) and optical density of the resultant solution was measured spectrophotometrically at 540 nm. The sGAG content of samples was extrapolated from a standard curve plotted from the optical density values of standard solutions of chondroitin sulphate from shark cartilage (concentration range: $0\text{-}100 \text{ }\mu\text{g mL}^{-1}$). The sGAG content for each sample was then normalised to the weight of blank Si80-CL or PCL scaffold measured on day 0. Results were expressed as mean \pm standard deviation. Statistical analysis. 2-tailed T-test was performed. Results were deemed significant if the probability of occurrence by random chance was less than 5% (i.e. $p < 0.05$).

Supplementary Figures

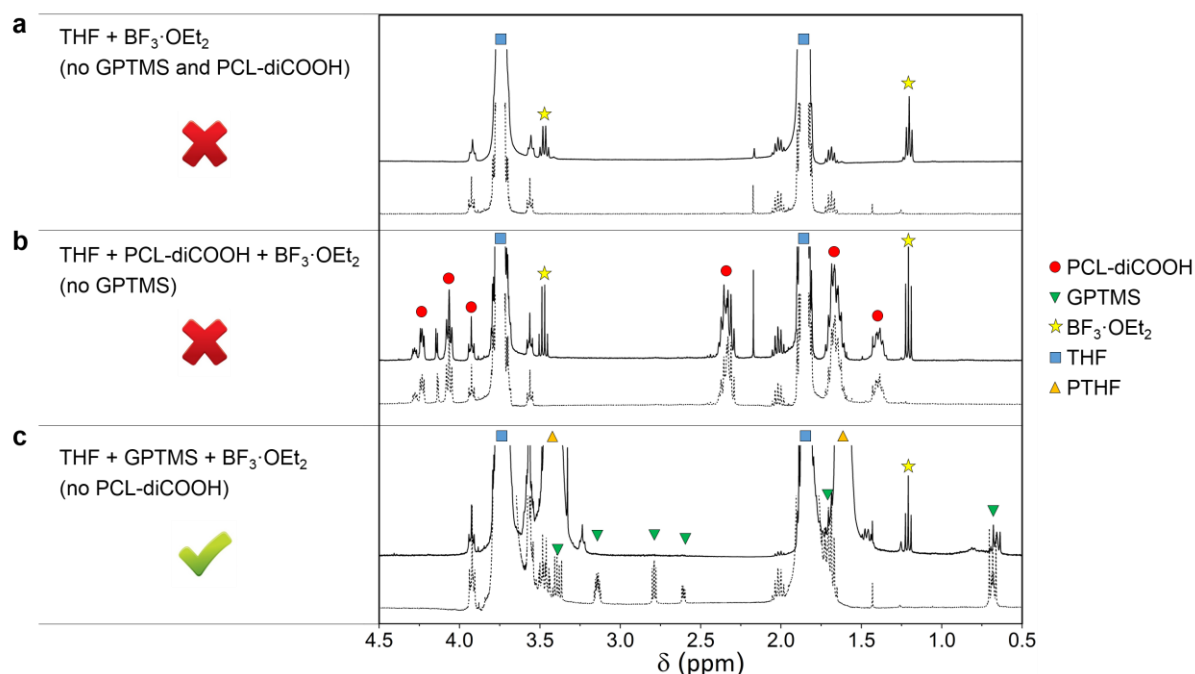


Figure S1

Evaluation of THF ring-opening polymerisation through liquid proton nuclear magnetic resonance ($^1\text{H-NMR}$): based on the fact that the addition of $\text{BF}_3\cdot\text{OEt}_2$ to the solution containing THF, GPTMS and PCL-diCOOH catalyses the polymerisation of the solvent, further $^1\text{H-NMR}$ analyses were run to give evidence of the influence of GPTMS and PCL-diCOOH on the mechanism of reaction. Three systems were considered (left column) and $^1\text{H-NMR}$ spectra were acquired before (dashed line) and after (solid line) $\text{BF}_3\cdot\text{OEt}_2$ addition (right column); THF polymerisation was verified from the appearance of the peaks typical of PTHF at $\delta = 1.62$ and 3.41 ppm. THF polymerisation was not catalysed by $\text{BF}_3\cdot\text{OEt}_2$ only (a), regardless of the presence of PCL-diCOOH (b). Only system c gave evidence of formation of PTHF, showing that it requires the co-presence of GPTMS and $\text{BF}_3\cdot\text{OEt}_2$ but it does not need PCL-diCOOH (c). Singlet at $\delta = 2.17$ ppm visible in some spectra is due to acetone residue from cleaning of the NMR tube.

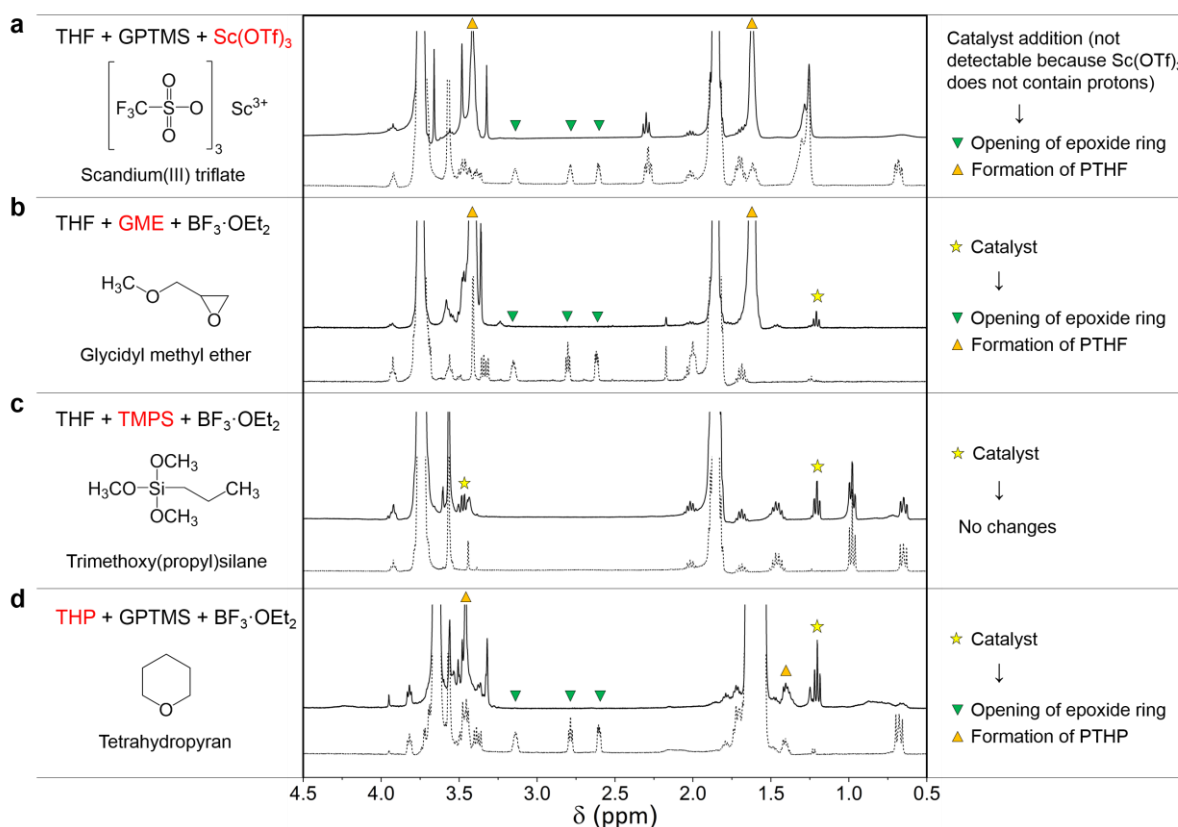


Figure S2

Examples of ring-opening polymerisation in alternative tri-component systems: in the system composed of THF-GPTMS- $\text{BF}_3 \cdot \text{OEt}_2$, one reagent at a time was substituted by another one with similar functionalities to check if the ring-opening polymerisation still occurred: **a**, Scandium(III) triflate ($\text{Sc}(\text{OTf})_3$) instead of $\text{BF}_3 \cdot \text{OEt}_2$ as catalyst. **b**, Glycidyl methyl ether (GME) instead of GPTMS as source of epoxide ring. **c**, Trimethoxy(propyl)silane (TMPS) instead of GPTMS as silica source without epoxide moiety. **d**, Tetrahydropyran (THP) instead of THF as cyclic monomer. For each change: the corresponding chemical formula is reported in the left column; central column shows the ^1H -NMR spectra before (dashed line) and after (solid line) the catalyst addition, with variations highlighted in the legend in the right column. Evidence of ring-opening polymerisation of the monomer was observed in the systems **a**, **b** and **d**, demonstrating that the reaction can occur from an alternative combination of a Lewis acid as catalyst (**a**), an initiator containing an epoxide ring (**b**) and a cyclic monomer containing at least one ring heteroatom (**d**). No changes were observed in system **c**, demonstrating that the silica moiety does not participate in the polymerisation reaction, although the presence of the silica functionality is essential to achieve the covalent bonding with the inorganic network in the hybrid system.

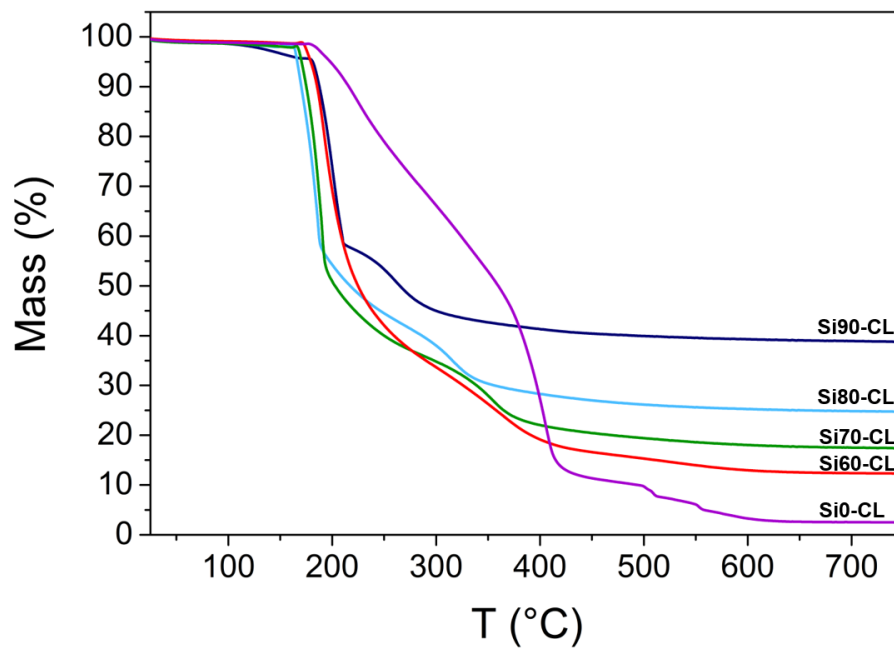


Figure S3

Evaluation of the I/O ratio: Mass loss of the five investigated hybrid compositions evaluated through thermal gravimetric analysis (TGA). The percentage of mass burnt-out during the analysis corresponds to the actual organic wt.% of the hybrid sample, which increased when TEOS/PCL-diCOOH ratio decreased from 90/10 (Si90-CL) to 0/100 wt.% (Si0-CL).

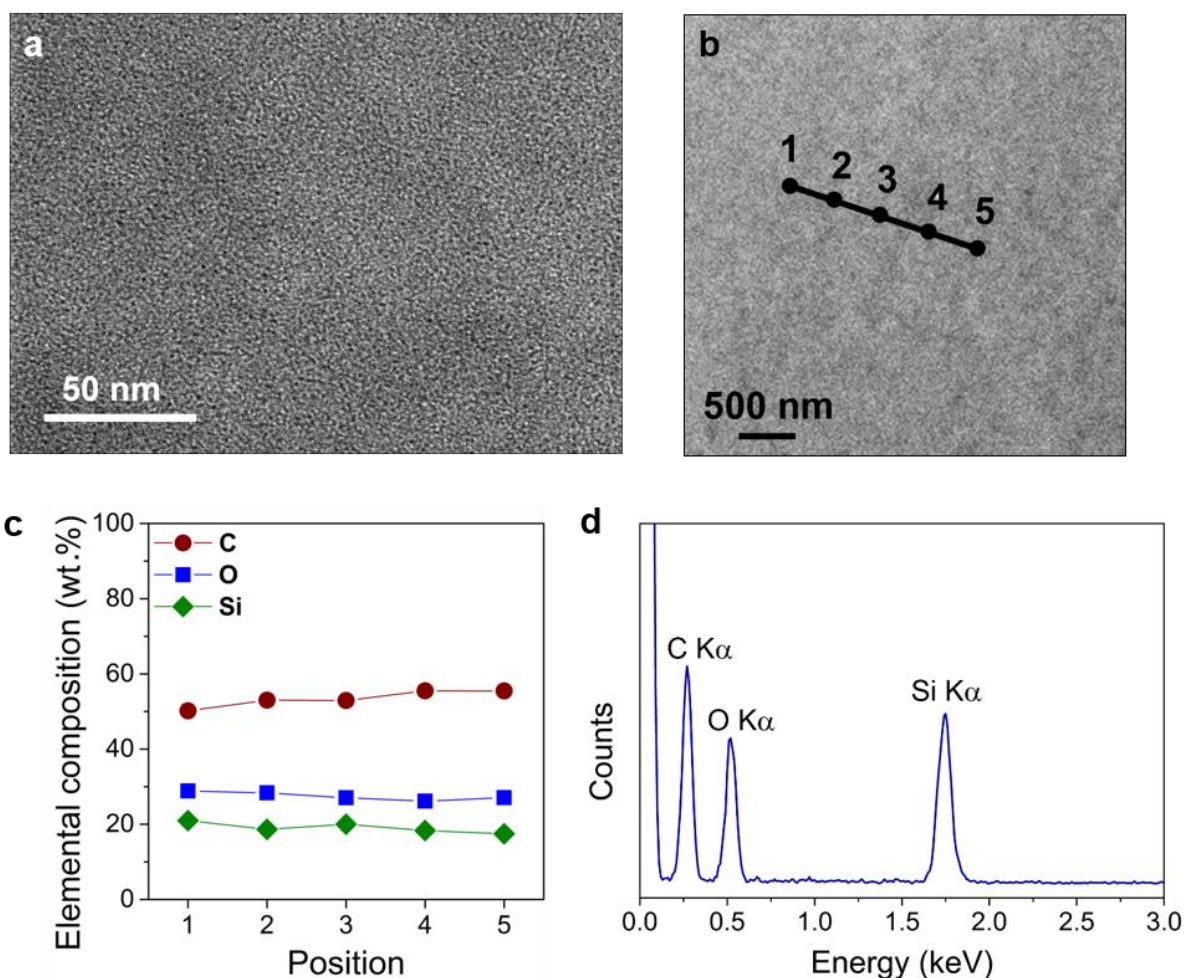


Figure S4

High resolution electron microscopy characterisation of the hybrid network on Si80-CL sample:

a, Bright field transmission electron microscopy (BFTEM) image; and **b**, High angle annular dark field - scanning transmission electron microscopy (HAADF-STEM) image of a section of a Si80-CL bulk sample. HAADF-STEM is a Z (atomic number) contrast imaging technique, i.e. higher the atomic number, the brighter the image contrast: brightness variations will be observed if the specimen has a non-uniform elemental composition. **c**, Semi-quantitative elemental ratio (C, O, Si) from scanning transmission electron microscopy - electron dispersive X-ray (STEM-EDX) spectrometry analysis on the five points on the line marked in **b**, showing carbon (organic) and silica presence and little change across the area analysed. **d**, Typical STEM-EDX spectrum showing the $K\alpha$ lines of C, O and Si at energy values of 0.277 keV, 0.525 keV and 1.740 keV, respectively. All these results confirmed the uniformity of the hybrid network at the nanoscale.

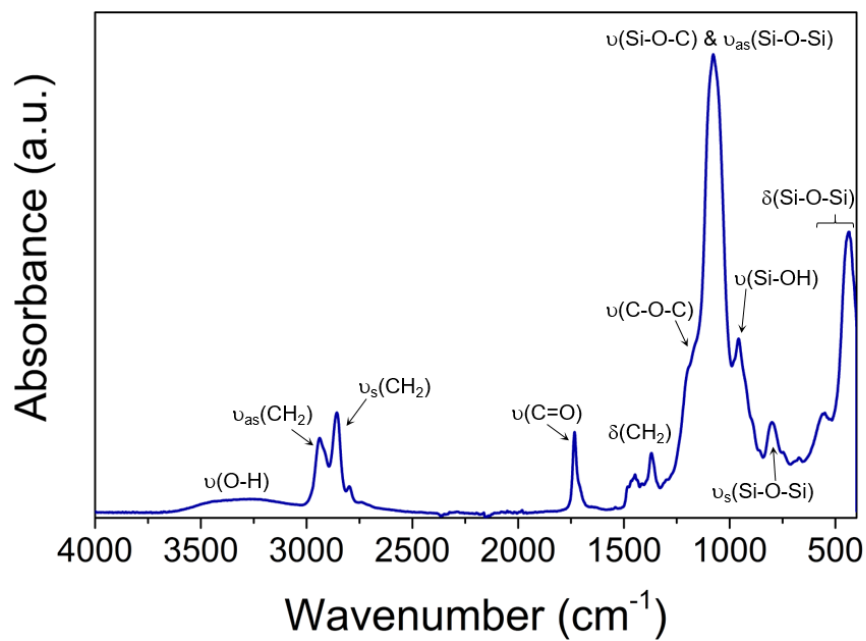


Figure S5

FTIR characterisation of the hybrid network on Si80-CL sample: typical ATR-FTIR (Fourier-transform infrared spectroscopy in attenuated total reflectance mode) spectrum, showing the co-presence of SiO_2 ^{8S}, PTHF^{9S} and PCL-diCOOH^{10S, 11S}.

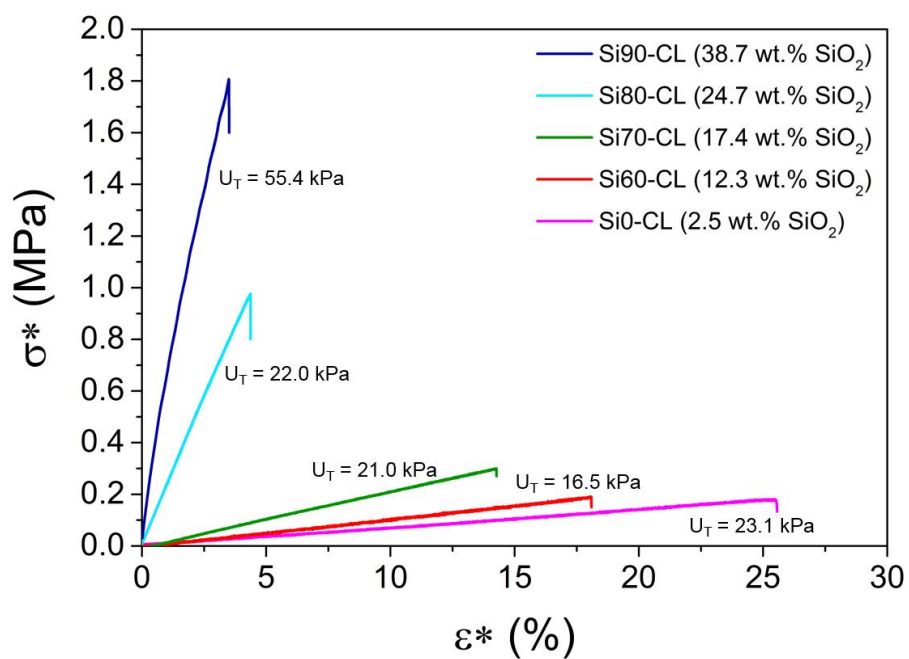
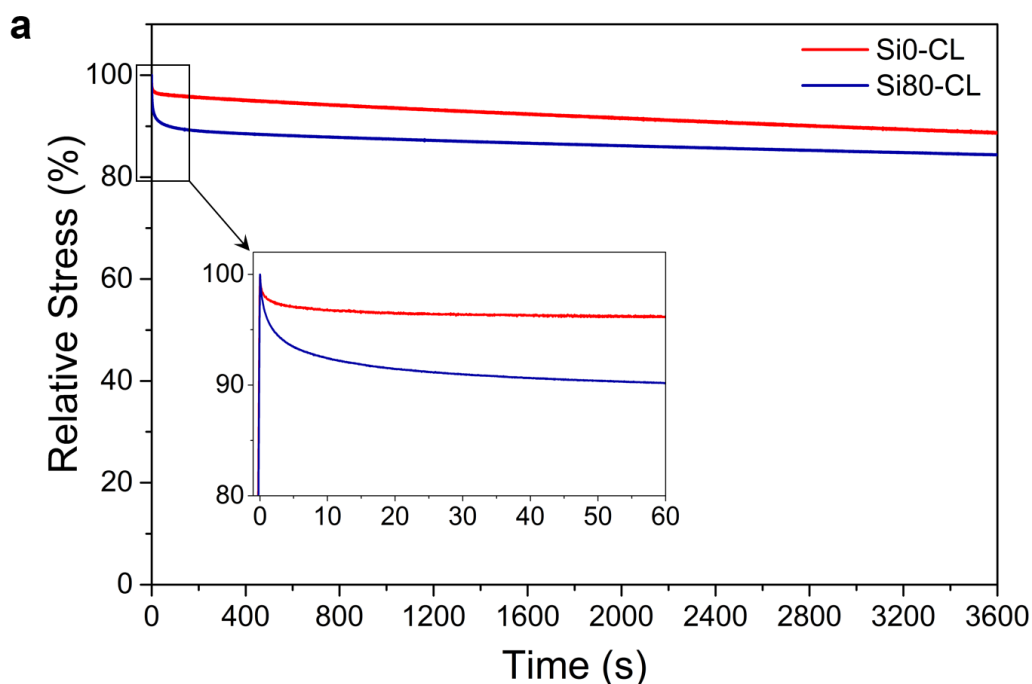


Figure S6

Tensile testing on hybrid monoliths: typical stress-strain curves (true values) up to failure for the five investigated compositions. Modulus of toughness (U_T), that represents the energy required to rupture a sample, was calculated for the five samples and the results match the values of strain and stress at failure reported in Fig. 2d, as toughness is a combination of these two properties. Since the inorganic component provides rigidity and ability to withstand high stress, the decrease in SiO₂ content led to an increase of fracture strain but also to a large decrease of fracture stress.



b

Time (s) *	Stress Loss (%)	
	Si0-CL	Si80-CL
5	1.9 ± 0.8	6.0 ± 0.6
60	2.9 ± 1.0	9.3 ± 1.0
300	3.8 ± 1.0	11.1 ± 1.3
1800	7.2 ± 1.0	13.7 ± 1.6
3600	10.5 ± 0.9	15.3 ± 1.7

* Time elapsed after application of stress

Figure S7

Stress-relaxation testing on hybrid monoliths: **a**, Typical stress-relaxation curves in tension of Si0-CL and Si80-CL samples (relative to the initial stress applied). **b**, Stress loss values at 5 s, 1 minute, 5 minutes, 30 minutes and 1 h relaxation for Si0-CL and Si80-CL compositions. The results show a small stress loss to a maximum value of ~11% and ~17% for Si0-CL and Si80-CL, respectively, after 1 h. These observations confirmed that the hybrid materials possess good mechanical stability, despite their self-healing ability. Stress-relaxation of self-healing systems is sometimes analysed with simple Zener model (also called “modified Maxwell”)¹²⁵, but this model does not fit well the data collected on the Si0-CL and Si80-CL samples, due to the probable presence of several relaxation mechanisms. The results suggest the presence of a very rapid relaxation followed by a more long term one, consistent with the complexity of the hybrid network (Fig. 1d). Further investigation would be needed to assess the nature of those mechanisms.

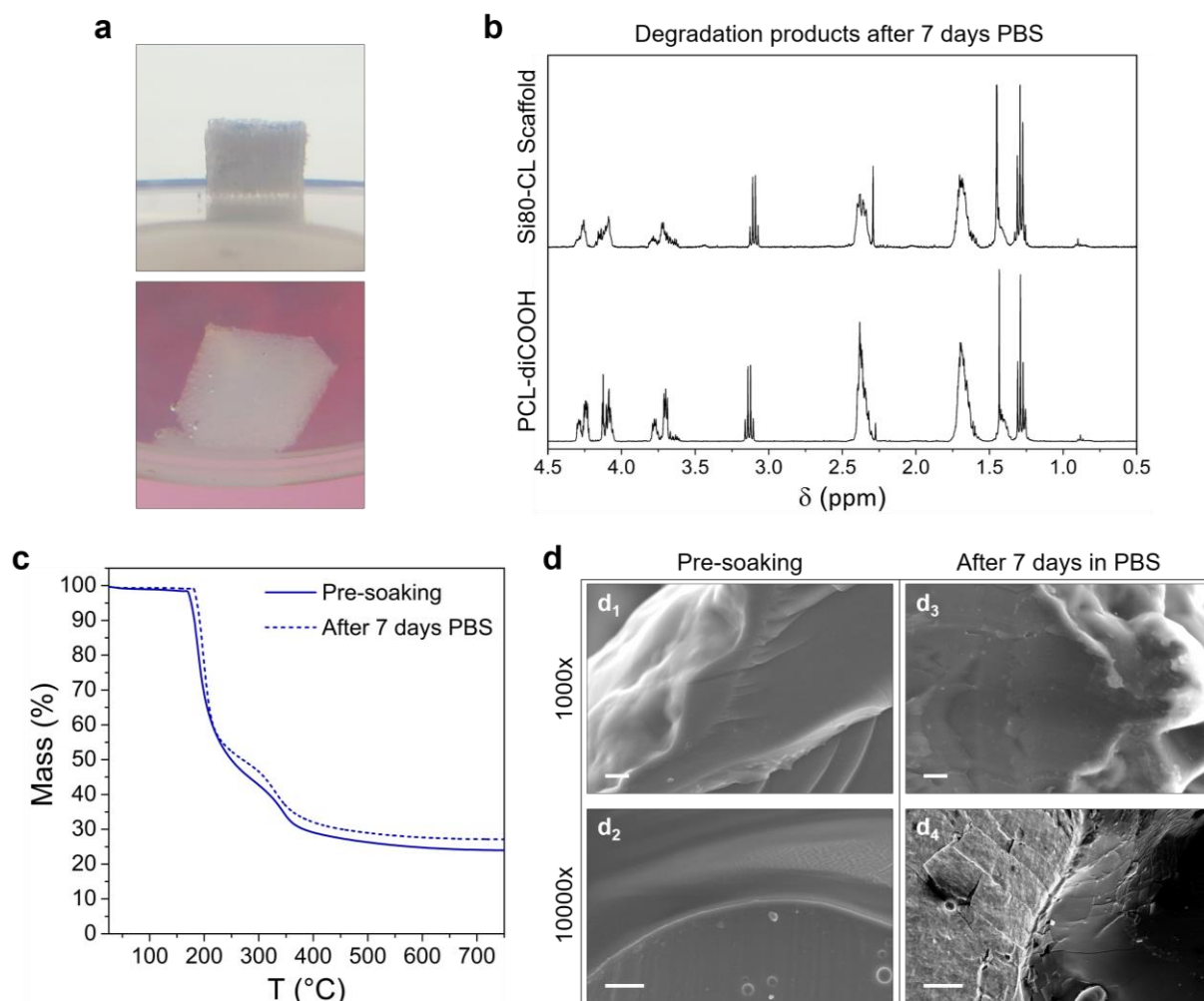


Figure S8

Biodegradation of Si80-CL scaffolds in PBS: **a**, Photographs of 3D printed Si80-CL scaffolds during immersion in PBS solution (7 days), which show no visible changes (swelling or cracking); **b**, $^1\text{H-NMR}$ spectra in CDCl_3 of the degradation products collected following immersion of a Si80-CL scaffold (top) and PCL-diCOOH (bottom) in PBS for 7 days. The spectrum collected on Si80-CL scaffold degradation products included all the peaks typical of PCL-diCOOH degradation products, while no PTHF was detected (reference spectra are in Fig. 1b). Triplet, singlet and quartet at $\delta = 1.29$, 1.44, 3.11 ppm, respectively, are due to contamination; **c**, TGA of the scaffold before (“Pre-soaking”) and after immersion in PBS (“After 7 days PBS”), showing I/O ratio increase from 23.8/76.2 wt.% (pre-soaking) to 27.0/73.0 wt.% (post-soaking), corresponding to a total mass loss of 12 wt.% due to the 7 days immersion, which was all organic. **d**, SEM images of Si80-CL scaffolds before (**d_1** and **d_2**) and after (**d_3** and **d_4**) 7 days immersion in PBS; **d_1** , **d_3**) cross-section of a strut (scale bar = 10 μm); **d_2** , **d_4**) external surface (scale bar = 2 μm).

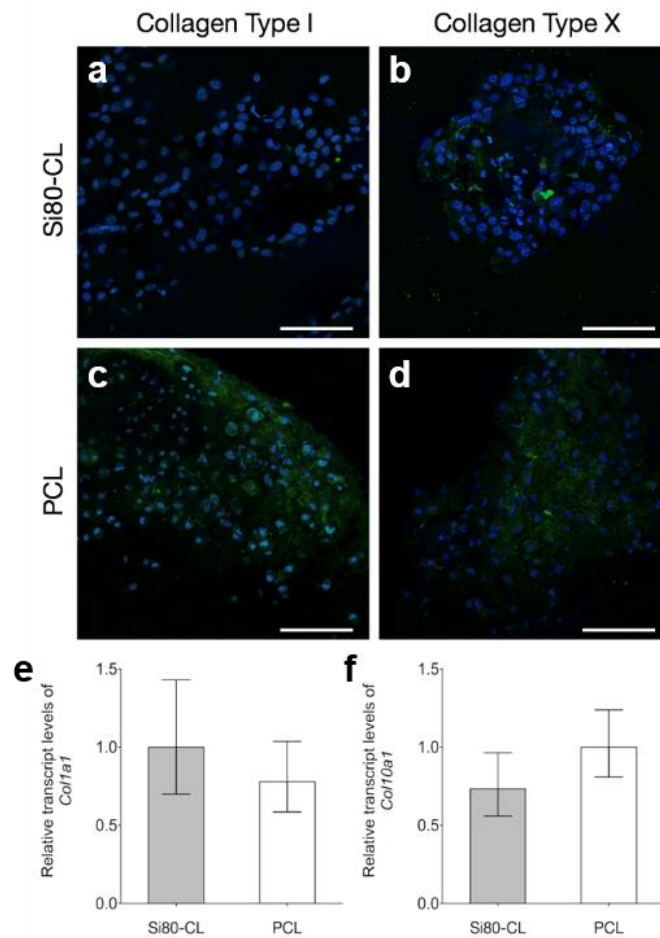


Figure S9

Supplementary in vitro cell studies on Si80-CL and PCL scaffolds: Analysis of day-21 cell seeded Si80-CL and PCL scaffolds. Immunohistochemistry (a-d) and qPCR (e-f) results suggested negligible expression of fibrocartilage marker Collagen Type I (*Col1a1*) and hypertrophic cartilage marker Collagen Type X (*Col10a1*). n = 3. Error bars in e and f represent range (upper and lower limits) of relative gene expression. Scale bar in a-d = 100 μ m.

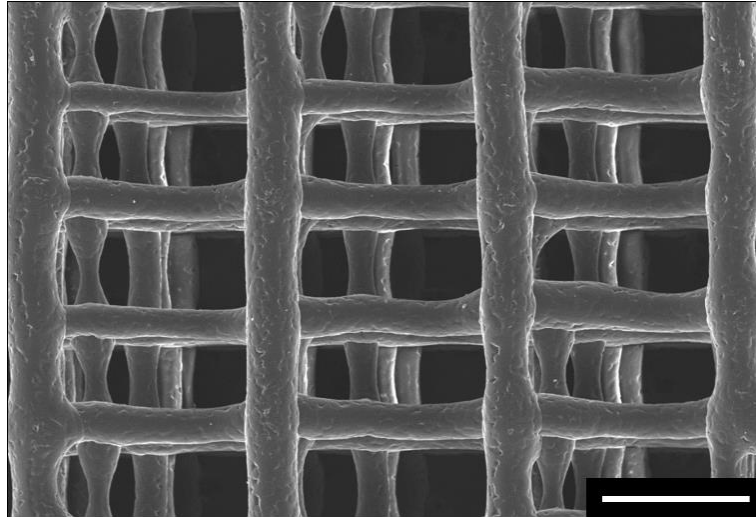


Figure S10

Morphology of PCL scaffolds: SEM image of the top surface of a reference PCL scaffold, characterised by struts of diameter $\sim 200 \mu\text{m}$ and rectangular channels ($\sim 250 \mu\text{m} \times \sim 600 \mu\text{m}$). Scale bar = $500 \mu\text{m}$.

Supplementary Videos

Video S1

Bouncing glass-based hybrid material: Example of bouncing of a Si80-CL cylindrical monolith. Slow-motion is used in order to better visualise the fast bouncing.

Video S2

Self-healing of glass-based hybrid material: Example of self-healing at room temperature of a Si0-CL sample (containing 2.5 wt.% SiO₂). A rectangular specimen was cut in halves with a sharp blade, the fractured pieces were quickly brought back together and the sample was able to recover its original shape.

Video S3

3D printing of porous scaffolds: Example of 3D extrusion printing directly from the sol-gel of a Si80-CL scaffold following a grid-like pattern with aligned 90° layers.

Supplementary References

- 1S. ASTM D1708-13, *Standard Test Method for Tensile Properties of Plastics by Use of Microtensile Specimens*, ASTM International, 2013.
- 2S. S. Yue, P. D. Lee, G. Poologasundarampillai, Z. Yao, P. Rockett, A. H. Devlin, C. A. Mitchell, M. A. Konerding and J. R. Jones, *J. Mater. Sci. Mater. Med.*, 2010, **21**, 847-853.
- 3S. S. Yue, P. D. Lee, G. Poologasundarampillai and J. R. Jones, *Acta Biomater.*, 2011, **7**, 2637-2643.
- 4S. A. L. B. Maçon, T. B. Kim, E. M. Valliant, K. Goetschius, R. K. Brow, D. E. Day, A. Hoppe, A. R. Boccaccini, I. Y. Kim, C. Ohtsuki, T. Kokubo, A. Osaka, M. Vallet-Regí, D. Arcos, L. Fraile, A. J. Salinas, A. V. Teixeira, Y. Vueva, R. M. Almeida, M. Miola, C. Vitale-Brovarone, E. Verné, W. Höland and J. R. Jones, *J. Mater. Sci. Mater. Med.*, 2015, **26**, 1-10.
- 5S. S. Li, B. G. Sengers, R. O. Oreffo and R. S. Tare, *J. Biomater. Appl.*, 2015, **29**, 824-836.
- 6S. A. M. Mackay, S. C. Beck, J. M. Murphy, F. P. Barry, C. O. Chichester and M. F. Pittenger, *Tissue Eng.*, 1998, **4**, 415-428.
- 7S. T. D. Brown, P. D. Dalton and D. W. Huttmacher, *Adv. Mater.*, 2011, **23**, 5651-5657.
- 8S. X. Zhang, Y. Wu, S. He and D. Yang, *Surf. Coat. Technol.*, 2007, **201**, 6051-6058.
- 9S. J. Zhang, Y. Niu, C. Huang, L. Xiao, Z. Chen, K. Yang and Y. Wang, *Polym. Chem.*, 2012, **3**, 1390-1393.
- 10S. S. Sahoo, A. Sasmal, R. Nanda, A. R. Phani and P. L. Nayak, *Carbohydr. Polym.*, 2010, **79**, 106-113.
- 11S. T. Elzein, M. Nasser-Eddine, C. Delaite, S. Bistac and P. Dumas, *J. Colloid Interface Sci.*, 2004, **273**, 381-387.
- 12S. J. J. Cash, T. Kubo, D. J. Dobbins and B. S. Sumerlin, *Polym. Chem.*, 2018, **9**, 2011-2020.